4
Methods and Algorithms of Searching for Thermodynamic Equilibria

A small boy asked the mathematician: "How much is twice two?" The mathematician said that he would think and after three days of thinking he shared his joy with the boy: "I have proved that this problem has a solution!"

A joke

4.1. E.G. Antsiferov's General Two-Stage Technique of Searching for Extreme Concentrations

As was noted in Section 2.4, even if we managed to strictly prove reducibility of the problem solved by MEIS to the convex programming (CP) problem, the difficulties caused by the setting of constraints on monotone change of thermodynamic functions presented in implicit form remain. E.G. Antsiferov [4, 7, 8] suggested a two-stage technique of searching for the vector of extreme concentrations x^{ext}. According to his idea, the surface of the thermodynamic function level that contains the point x^{ext} is determined at the first stage, coordinates of this point are sought on this surface at the second stage.

The first stage is based on the analysis of possible locations of the point x^{ext} in the thermodynamic attainability region $D_t(y)$ relative to the points y and x^{eq}. This stage was described in Section 2.4 (see Fig. 2.9).

Different cases are considered in the search for extreme concentration point x^{ext}. The first situation is the case of *monotone decrease of Gibbs energy* (or another characteristic function) on the interval segment $[y, x^{\text{mat}}]$. In this case the second stage is excluded (Fig. 2.9*a*), since the point x^{mat} proves to be a solution to the problem of searching for x^{ext}. The first stage reduces to solution of the canonical linear programming (LP) problem (nonlinear thermodynamic constraints do not influence the location of x^{ext}).

The second situation is the case of *continuous increase of the function* $G(x)$ on the segment y, x^{mat} (Fig. 2.9*b*). In this case the canonical CP problem (2.116) is solved at the second stage.

The third situation is the case of the *minimum point of* $G(x)$ (the thermodynamic "pothole") on the segment $[y, x^{\text{mat}}]$ (Fig. 2.9*c*). This point is taken as the sought

TABLE 4.1. Calculation results of hexane isomerization ($T = 600$ K, $P = 0.1$ MPa)

Substance	Gibbs energy kj/mole, kJ/kg	State			
		y mole/kg, kg/kg	x^{eq}, mole/kg, kg/kg	x^{mat}, mole/kg, kg/kg	x^{mat}, mole/kg, kg/kg
x_1	−421.034	11.60	3.283	0	1.042
(isomer 1)	−4886	1.00	0.283	0	0.090
x_2	−423.620	0	5.513	11.60	9.670
(isomer 2)	−4916	0	0.475	1.00	0.833
x_3	−420.255	0	2.808	0	0.892
(isomer 3)	−4877	0	0.242	0	0.076
$L = \sum_j c_j x_j$, mole/kg,		0	5.513	11.60	9.670
G, kJ/kg		−4885.7	−4958.8	−4915.7	−4942.8
H, kJ/kg		−1294.0	−1294.0	−1321.0	−1313.0
S, kJ/(kg·k)		6.066	6.006	5.991	5.996
υ,m^3/kg		0.571	0.571	0.571	0.571
ρ,kg/m^3		1.750	1.750	1.750	1.750
x, mole/kg,		11.60	11.60	11.60	11.60

Situation: a thermodynamic "pothole."

level of $G(x^{ext})$, and the CP problem (2.118) is solved. The function $G(x^{ext})$ in this situation is determined with some error, as we discussed in Section 3.2 (see Figs. 2.4 and 3.1*a*).

In order to solve the CP problems at the second stage of searching for x^{ext} Antsiferov developed some algorithms on the basis of methods of the support cone, affine scaling, and generalized linear programming [4, 83]. The further MEIS-based studies of thermodynamic problems were performed using both modified and newly developed algorithms. However, the two-stage scheme of determining x^{ext} by Antsiferov remained invariable [81, 83, 102].

The scheme is highly attractive in terms of the analysis of results of thermodynamic computations as well. It allows their representation in a convenient tabular form, which is illustrated again on the example of hexane isomerization. The data on this process in Table 4.1 describe its thermodynamic features fully enough.

Conditions for attaining the sought extreme concentration ($\max x_2$) are determined from the figures in the columns under "State" and in the footnote "Situation." The case of the thermodynamic "pothole" takes place here. Yield of x_2^{ext} is approximately 80% higher than x_2^{eq} and turns out to be more than 10% lower than x_2^{mat}. The absolute value of difference $|x_2^{mat} - x_2^{ext}|$ is the value that cannot be exceeded by the error in calculation of x_2^{ext}, i.e., it is a very rough estimation of solution accuracy. Comparison of the standard values of free enthalpy in the column "Gibbs energy" reveals competitiveness of individual components of the reaction mixture in the contest for a place in the final equilibrium composition. The values of thermodynamic parameters in the lower part of Table 4.1 describe the properties of system states considered in the computation process.

Numerous calculations of most diverse systems (technical and natural) demonstrated high efficiency of the algorithm of stage 1 of Antsiferov's scheme. The results were always logically consistent. In rare cases, when it was possible to *estimate* calculation accuracy more correctly than to find them by comparison between values of x^{ext} and x^{mat}, the estimates were acceptable. This does not mean, however, that in the future one will not run across such situations where the errors in determining $G(x^{\text{ext}})$ will be impermissibly large. Therefore, the problem of devising alternative methods of searching for x^{ext} is topical. Construction of algorithms on the basis of the idea of a thermodynamic tree seems to be a possible alternative to Antsiferov's scheme.

The next Sections of this chapter dwell on algorithms for determination of y^{ext} and x^{ext} (stage 2 of calculations made using Antsiferov's technique) and the alternative algorithm for determination of $G(x^{\text{ext}})$ based on the idea of the thermodynamic tree (stage 1 of calculations made using Antsiferov's technique). The last section, Section 4.5, presents preliminary considerations on the technique for estimating feasibility and stability of the partial equilibria of x^{ext}.

4.2. Optimization of the Initial Composition of Reagents in a Chemical System by the Simplex Embedding Method

It is difficult to apply MEIS (2.43)–(2.50) of systems with a variable initial composition of reagents for choosing an optimal value of y because, in the problem statement, the vectors x and y are analytically independent. Therefore, it is complicated to apply methods requiring that functions and their derivatives—ones that depend simultaneously on the values of these two vectors—be calculated in the iterative process.

To solve a general problem of searching for the point $(x^{\text{ext}}, y^{\text{ext}})$ E.G. Antsiferov applied the *simplex embedding method* to determine y^{ext} [6].

The simplex belonging to the Euclidean space R^n with the vertex at the point x_0 and the edges $x_1 - x_0, \ldots, x_n - x_0$, that form the basis in R^n is a polyhedron, all points of which satisfy the condition

$$x = x_0 + \sum_{i=1}^{n} \alpha_i (x_i - x_0), \quad \sum_{i=1}^{n} \alpha_i \leq 1, \ \alpha_i \geq 0. \tag{4.1}$$

Without loss of generality it is assumed that $x_0 = 0$, i.e., x_0 coincides with the coordinate origin. The simplex volume is determined by the formula

$$V = \frac{[\det(x)]}{n}, \tag{4.2}$$

where x is an $n \times n$ matrix whose rows are the transposed vectors of coordinates of the vertices. The simplex center is found from the expression

$$x_c = \frac{(x_0 + \cdots + x_n)}{(n+1)}. \tag{4.3}$$

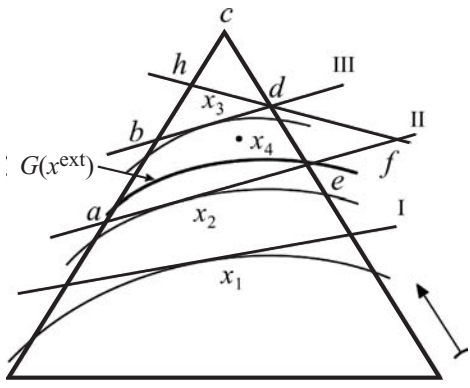

FIGURE 4.1. Geometrical interpretation of the simplex embedding method.

It is convenient to apply the simplex to computational procedures because its topology is so simple compared to other convex polyhedrons. In the simplex, edges connect each vertex every other one, this being another distinctive feature along with (4.1).

At $n = 0, 1, 2, 3$, the simplexes are, respectively, a point, a line segment, a triangle, and a tetrahedron. Note in addition that simplex vertices do not exist in one $(n-1)$-dimensional plane (where n is simplex dimension). Simplex faces are simplexes of lower dimensionality. A tetrahedron face is a triangle, a simplex of dimension $n = 2$, and so on.

The idea of the simplex embedding method consists in sequential construction of simplexes containing the point $x^{\text{ext}}(y)$. The volume of each subsequent polyhedron turns out to be less than the volume of the preceding one and the solution is progressively localized. The monotone decrease in volumes provides convergence of computations.

The algorithm scheme is explained in Fig. 4.1. It presents the region boundary for admissible solutions of $D_t(y)$ (the bold curve), four simplexes, corresponding to calculation iterations, with simplex centers and the truncating planes used to construct simplexes.

First the simplex with the center x_1 is constructed. Since the objective function $(\sum_j c_j x_j)$ increases toward the admissible region boundary (the direction of increase in Fig. 4.1 is shown by the arrow), it is possible to further localize a solution. To do this, we draw truncating plane I through x_1 or somewhat above it. The plane isolates the simplex with center x_2, in which the objective function value lies higher than in simplex with center x_1. The center of the third simplex x_3 finds itself in the inadmissible region. When we draw the truncating plane III through it, a zone of further search for the solution by the polyhedron *abdea* is limited. For its substitution by the simplex, the segment *bc* is divided in two and a straight line is drawn from the obtained point *h* through the point *d* to the intersection of *f* with the truncating plane II.

The center x_4 of the fourth simplex *ahfa* is now located close to the admissible region boundary and the point with the extreme concentration x^{ext} of desired products of a process that lies on it.

As is seen from equation (4.1), the simplex embedding method requires that the problem constraints be set as non-homogeneous inequalities. Conditions (2.47), which determine admissible relations among the $y$vector components, can apparently be rewritten in the form

$$\sum_{j=1}^{l} \alpha_{kj} y_j \leq 0,\ k \in K. \tag{4.4}$$

To pass from (4.4) to nonhomogeneous inequalities, some variable, the first, for example, will be expressed through the remaining ones based on the normalization condition (2.44):

$$y_1 = 1 - \frac{\sum\limits_{j=2}^{l} M_j y_j}{M_1}. \tag{4.5}$$

Then the initial simplex is determined by the obvious inequality

$$\sum_{j=2}^{l} \frac{M_j}{M_1} y_j \leq 1, \tag{4.6}$$

where all $\frac{M_j}{M_1}$ are strictly greater than zero.

The truncating plane is constructed using the solution $(\bar{x})$ of the following CP problem:

Find

$$\max \sum_{j=1}^{n} c_j x_j \tag{4.7}$$

subject to

$$Ax = b\,(y_c) = \sum_{j=1}^{n} y_j A_j, \tag{4.8}$$

$$G\,(x) = \overline{G}\,(y_c)\,, \tag{4.9}$$

$$x_j > 0, \tag{4.10}$$

where y_c and $\bar{G}(y_c)$ are the simplex center and the associated Gibbs energy level, respectively, and A_j is the jth column of the matrix A. The solution $\bar{x}$ along with (4.8)–(4.10) satisfies the Kuhn–Tucker conditions:

$$c_j = \sum_{i=1}^{m} \lambda_i a_{ij} + \lambda_{m+1} \nabla_j G\,(\bar{x})\,, \tag{4.11}$$

$$\lambda_{m+1} > 0, \tag{4.12}$$

where $\nabla_j G(\bar{x})$ is the jth component of the gradient $G(x)$ at the point $\bar{x}$.

Let us increase the initial component y_c by a small value Δy. This will involve a change in the material balances (4.8), and the relation (4.9):

$$G\,(x) \leq \bar{G}\,(y_c)\,.$$

The optimal solution $\bar{x}$ and the objective function (4.7) will also change. The former will increase by Δx and the latter by $c\Delta x$. If Δy is chosen to be rather small, the set of active constraints and the dual solution to problem (4.7)–(4.10) will remain invariable.

In a linear approximation variation of the solution, Δx will satisfy the conditions:

$$A\Delta x = \sum_{j=1}^{l} \Delta y_j A_j, \tag{4.13}$$

$$\nabla^T G(\bar{x})\,\Delta x = \nabla^T \bar{G}(y_c)\,\Delta y. \tag{4.14}$$

If we multiply equality (4.13) by λ_i, $i = 1, \ldots, m$, equality (4.14) by λ_{m+1}, add the results, and take into consideration (4.11), the objective function (4.7) will be

$$\Delta F = \sum_{j=1}^{l} \left[\sum_{i=1}^{m} \lambda_i a_{ij} + \lambda_{m+1} \nabla \overline{G}(y_c) \right] \Delta y_j. \tag{4.15}$$

Based on (4.11) the formula for the truncating half-space in the y variables can be written:

$$d^T (y - y_c) \geq 0, \tag{4.16}$$

where

$$d_j = \frac{a_j}{\Psi(y_c)} - \frac{\left(c^T \bar{x}\right)}{\Psi(y_c)^2}, \tag{4.17}$$

$$a_j = \sum_{i=1}^{m} \lambda_i a_{ij} + \lambda_{m+1} \nabla \bar{G}(y_c), \tag{4.18}$$

$$\Psi(y_c) = \sum_{j \in J_c} y_j. \tag{4.19}$$

This algorithm can check admissibility of a simplex center at each iteration in terms of yield of substances of interest to the researcher.

4.3. Calculations of Complete and Partial Equilibria by the Affine Scaling Method

The point of the final equilibrium x^{eq} on the material balance polyhedron $D(y)$ is sometimes sought by the Lagrange multipliers method (see, for example, [9]. The system of equations obtained in this case by equating the partial derivatives of L to zero is solved by the Newton method or some other method. Such an approach is suitable when x^{eq} is an interior point of $D(y)$. However, in Chapter 2 it was shown that this condition is not fulfilled when the thermodynamic system contains condensed phases. Besides, the method of multipliers is difficult to apply when inequality constraints are included in the models of final equilibria.

Applicability of the multipliers method to calculate x^{ext} (model (2.38)–(2.42)) becomes even more problematic than searching for x^{eq} because of the necessity to consider a wide diversity of constraints. Therefore, we applied solely the MP methods for searching for x^{eq} and x^{ext} [1]. Here we will dwell on the affine scaling method that has been used most often so far in studies on thermodynamic attainability regions and partial equilibria [34, 35].

The affine scaling method is convenient because it handles only the interior points of $D(y)$, in which an objective function gradient can be calculated and the motion to the extremum point is executed at an acute angle to this gradient taken with the opposite sign. The latter circumstance facilitates convergence of the method at an unfavorable (with the zones of small steepness) surface shape, on which the extremum point is sought. Using the figurative comparison we will explain that when descending the mountain by this method we determine motion direction not by touch, as in the steepest descent method, but by choosing the lowest point in the visible vicinity and adjusting the route after reaching it.

The idea of the above method will be illustrated with the example of searching for the point x^{eq}. An initial point for the computational process is some interior point x^0 of the polyhedron $D(y)$, at which $x_j^0 > 0$ for all $j = 1, \ldots, n$. At each iteration $k = 0, 1, 2, \ldots$, the obvious conditions on conservation of the mole quantities of elements and their positiveness are assumed:

$$\sum_{j=1}^{n} a_{ij} \left(x_j - x_j^k\right) = 0, x_j^k > 0. \tag{4.20}$$

The correction vector $z = (z_1^k, \ldots, z_n^k)^T$ whose components are $(x_j - x_j^k)$ determines direction of the motion at the kth iteration.

The ellipsoid is constructed with center at x^k such that

$$\sum_{j=1}^{n} \frac{z_j^2}{(x_j^k)^2} \leq 1, \tag{4.21}$$

which represents a "visible vicinity." This means the ellipsoid axes are distances from x^k to the positive orthant boundaries that determine a "visibility zone" subject to (4.20).

The point with the minimum Gibbs energy is sought by the linearization technique, i.e., the partial derivatives of the function $G(x)$ are calculated as

$$g_j^k = \frac{\partial G\left(x^k\right)}{\partial x_j}, \tag{4.22}$$

[1] Indicating the problems in application of the multipliers method, we mean its application as the basic procedure of computational algorithms. As an auxiliary procedure this method is included in many MP algorithms.

and the minimum value of the linear form is determined to be

$$C = \sum_{j=1}^{n} g_j^k z_j \tag{4.23}$$

subject to

$$\sum_{j=1}^{n} a_{ij} z_j = 0, \tag{4.24}$$

$$\sum_{j=1}^{n} \frac{z_j^2}{\left(x_j^k\right)^2} = 1. \tag{4.25}$$

As compared to (4.21) the strict equality sign is used in (4.25), since the linear function reaches its minimum at the boundary point of the convex set, in this case on the ellipsoid surface or the plane of its intersection with the material balance polyhedron.

The solution z of problem (4.23)–(4.25) is found using the system of equations obtained as a result of equating partial derivatives of the Lagrange functions (4.26) to zero:

$$L(z, \lambda) = \sum_{j=1}^{n} g_j^k z_j - \sum_{i=1}^{m} \lambda_i \sum_{j=1}^{n} a_{ij} z_j + \lambda_{m+1} \left(1 - \sum_{j=1}^{n} \frac{z_j^2}{\left(x_j^k\right)^2} \right). \tag{4.26}$$

The solution thus is represented by the formulas

$$z_j = \left(x_j^k\right)^2 \frac{\sum_{i=1}^{m} \lambda_i a_{ij} - g_j^k}{2\lambda_{m+1}}, \tag{4.27}$$

$$2\lambda_{m+1} = \left(\sum_{j=1}^{n} \left(x_j^k\right)^2 \left(\sum_{i=1}^{m} \lambda_i a_{ij} - g_j^k \right)^2 \right)^{0.5}, \tag{4.28}$$

$$\lambda = g A^{-1}, \tag{4.29}$$

where λ is a vector of the Lagrange multipliers with material balance constraints that include m components of λ_i. The iteration k terminates when the interior point x^{k+1} is determined, at which the minimum of function $G(x)$ is reached on the segment that coincides with its direction and is equal to the absolute value of z.

The process is repeated, until the magnitude

$$F_k = 4\lambda_{m+1}^2 = \sum_{j=1}^{n} \left(x_j^k\right)^2 \left(\sum_{i=1}^{m} \lambda_i a_{ij} - g_j^k \right)^2 \tag{4.30}$$

becomes less than the given small number ε. The sense of a rule that interrupts the process is clear, since the negligibly low value of F_k is associated with the

negligibly low value of λ_{m+1} and hence, it is associated with quite an inessential change in the objective function with a change in ellipsoid parameters.

Transformation of system (4.26)–(4.30) results in an alternative statement of the problem on determination of the descent direction on the surface of $G(x)$:

Find

$$\min\left(\sum_{j=1}^{n} g_j^k z_j + 0.5\sum_{j=1}^{n}\frac{z_j^2}{x_j^{k2}}\right) \tag{4.31}$$

subject to

$$Az = 0. \tag{4.32}$$

To control the method of convergence, the magnitude z can be multiplied by the coefficient α , i.e., from the equation

$$x = x^k + z^k \tag{4.33}$$

it is possible to pass to the equation

$$x = x^k + \alpha^k z^k \tag{4.34}$$

where step size $\alpha^k z^k$ is chosen such that $x > 0$. Affine scaling method is illustrated graphically in Fig. 4.2*a* and *b*.

We seek the initial interior point x^0 (the point of introduction in the admissible region) by several specially developed algorithms. Let us consider two of them.

The first (I.I. Dikin's [34, 35]) algorithm applies the idea of the basic affine scaling method and solves the following problem:

Find

$$\min\sum_{j=1}^{n}\frac{z_j^2}{\left(x_j^k\right)^2} \tag{4.35}$$

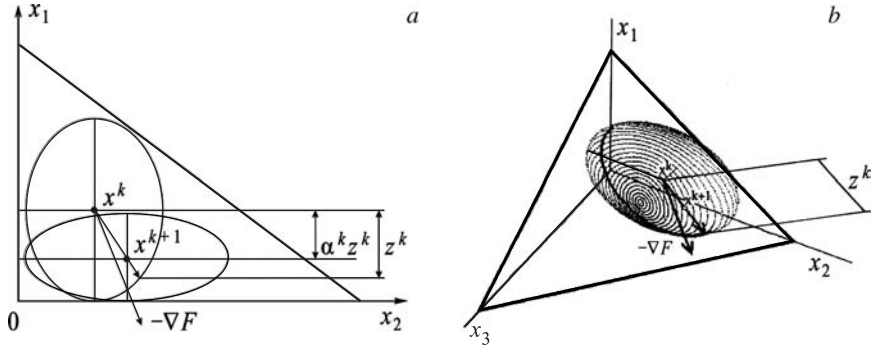

FIGURE 4.2. Graphical interpretation of the affine scaling method in (*a*) two- dimensional and (*b*) three-dimensional spaces.

subject to

$$Az = r^k, \tag{4.36}$$

where

$$r^k = b - Ax^k. \tag{4.37}$$

Transition from x^k to x^{k+1} is performed by equation (4.34), α^k is taken such that x^{k+1} belongs to the interior admissible region. The step size should not exceed unity, in this case. The calculation terminates when the absolute value of the imbalance $|r^k|$ becomes less than the given value ε .

Search for x^0 by the second (E.G. Antsiferov's) algorithm is based on the solution to the following auxiliary LP problem:

$$\left.\begin{array}{l} \text{Find} \\ \qquad \max \Delta \\ \text{subject to} \\ \displaystyle\sum_{j=1}^{n} a_{ij} y_j + \Delta \sum_{j=1}^{n} a_{ij} = b_i \;\; i = 1, \ldots, m,\; y_j \geq 0,\; \Delta > 0 \end{array}\right\} \tag{4.38}$$

Components of the vector x^0 are determined by the formula $x_j^0 = y_j + \Delta$. The second algorithm is apparently easier to apply then the first.

The solution of x^0 found by any of the mentioned algorithms can be additionally corrected based on the fact that all the interior points of the segment $[x^0, y]$ are the interior points of $D(y)$. For example, it seems logical to choose a minimum Gibbs energy point on this intercept as an initial approximation in the search for x^{eq}. The choice may contribute to an increase in the convergence rate of computations.

When the affine scaling method is used for searching for the point x^{ext}, the formulas to calculate the coefficients g_j in the objective function (4.23) change, and additional members on the right-hand side of equation (4.26) appear that correspond to constraints on the Gibbs energy values in the models of type (2.116) or (2.118). The general scheme of algorithm application, however, remains invariable.

Despite the fact that the affine scaling method proved to be highly efficient for solving a large number of applied thermodynamic problems, there are cases of extremely slow convergence such as in the solution of environmental problems, where the spread in values of the sought variables reaches 10–12 orders of magnitude and higher.

This problem was solved by I.A. Shirkalin [156]. He revealed a sharp deceleration of convergence of the discussed method near the point x^{eq} when concentrations of part of the reaction mixture components approach zero. In the search for a direction of optimal descent (z) he formulated the simplest two-dimensional problem, introducing three assumptions: 1) the initial point x^0 is close to the solution; 2) the objective function is strictly convex and twice continuously differentiable; 3) the value of the second coordinate (r) is much lower than that of the first (R).

Shirkalin determined the coordinates z by expansion of the objective function into the Taylor power series, $z = x - x^0$, and employed just the first three members

of the series, i.e.

$$F(x) = F\left(x^0\right) - (\nabla, z) + 0.5\left(\nabla^2 z, z\right), \tag{4.39}$$

where ∇ is an antigradient and

$$\nabla^2 = \left[\frac{\partial^2 F(x)}{\partial x_1, \partial x_2}\right]$$

is a Hessian matrix at the point x^0.

Based on the minimization of $F(x)$ Shirkalin determined that

$$z_1 \approx \nabla_1 \quad \text{and} \quad z_2 \approx -r. \tag{4.40}$$

Transition to formulas (4.40) in the affine scaling method was performed using the auxiliary model he constructed:

Find

$$\max\left(\nabla_1 z_1 + \nabla_2 z_2\right) \tag{4.41}$$

subject to

$$\frac{z_1^2}{R^{2\beta}} + \frac{z_2^2}{r^{2\beta}} = 1, \tag{4.42}$$

where β is a sought parameter of the method.

Solution to problem (4.41), (4.42) reduces to (4.40) at $\beta = 0.5$. This value of β was applied to accelerate convergence of the computational process, i.e., when approaching the point x^{eq} expression (4.25) was replaced in the procedure of transition from the kth to the $(k+1)$th iteration by the expression

$$\sum_{j=1}^{n} \frac{z_j^2}{x_j^k} = 1, \tag{4.43}$$

which may be interpreted as an ellipsoid equation with axes $x_j^{0.5}$.

Since β was determined on the basis of the expansion in (4.39), the algorithm applied by Shirkalin can be treated as a realization of the general Newton method for minimization problems:

$$x^{k+1} = x^k - \left[\nabla^2 f\left(x^k\right)\right]^{-1} \nabla f\left(x^k\right). \tag{4.44}$$

Under Shirkalin's assumptions fit to a physical nature of the problems discussed in the book, the Newton method shows fast convergence [94, 142]. This explains the efficiency of substituting the parameter $\beta = 0.5$ into the ellipsoid equation applied in the affine scaling method. The calculating advantages of Shirkalin's algorithm were confirmed by its application to the thermodynamic analysis of anthropogenic air pollution (see Chapter 5) and the solution of some other problems.

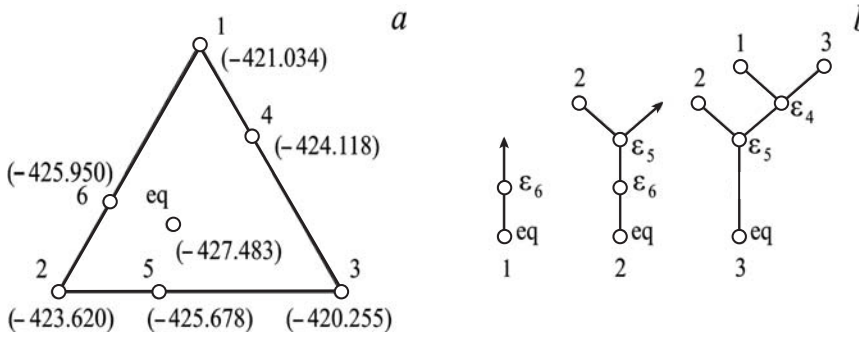

FIGURE 4.3. Construction of the thermodynamic tree of hexane isomerization reaction.

4.4. Construction of Algorithms Using the Thermodynamic Tree Idea

In this Section we present potential schemes of the algorithms for constructing a thermodynamic tree, whose efficiency was discussed briefly in Chapter 3. At first, consideration will be given to the exact algorithm described in *Equilibrium Encircling* [58] and then the algorithm will be explained on the examples of hexane isomerization and hydrogen combustion in oxygen of Section 3.2.

The tree construction for converting the isomers C_6H_{14} is illustrated in Fig. 4.3*a* and *b*. According to [58] we introduce the notation:

$D_0 = \{\upsilon_1, \ldots, \upsilon_l\}$is a set of the vertices of $D(y)$;
$D_1 = \{d_1, \ldots, d_k\}$is a set of the edges of $D(y)$;
ε_d is the minimum Gibbs energy value at the edge d.

First of all calculations, are made of the Gibbs energy values for all vertices υ and the minimum values of G (in kJ) at all edges ε_d. These values are presented in Fig. 4.3*a* (see, also, Fig. 3.1). The values ε_d are arranged in increasing order (ε_d may coincide with the Gibbs energy value at one of the vertices adjacent to the edge d).

The tree construction ("growth") starts with its root, i.e., the equilibrium point x^{eq}. Relative to x^{eq} the whole triangle 123 is the single component of arcwise connectedness, since there is a thermodynamically admissible path to x^{eq} from any of its points. We connect the point x^{eq} by the segment (the tree branch) with the point ε_6 that corresponds to the minimum Gibbs energy level from the calculated point ε_d (that maps the line $G(x) = \varepsilon_6$ within the appropriate component of arcwise connectedness). Relative to the point ε_6 the triangle part, for which $G(x) \geq \varepsilon_6$, is also the single component of arcwise connectedness. It results from the fact that all the triangle vertices are connected by edges (or a chain of edges), at which $\varepsilon_d > \varepsilon_6$, and hence, any point of the triangle with $G(x) \leq \varepsilon_6$ can be reached from any vertex by the thermodynamically admissible path. Thus, the point ε_6 is not a ramification

point and the line $x^{eq} - \varepsilon_6$ is extended to the next point ε_5 in increasing order of $G(x)$.

Relative to the level ε_5 there is vertex 2, which cannot be connected with other vertices by the edges with $\varepsilon_d > \varepsilon_5$. Therefore, part of the triangle between the line $G(x) = \varepsilon_5$ and vertex 2 is an arcwise connectedness component with respect to ε_5. The rest of the polyhedron $D(y)$ is another component. Hence, the point ε_5 is a branch point. One branch of the tree connects it with the end vertex 2 and another leads to the next in increasing order of $G(x)$ at the point ε_4.

Relative to the level ε_4 none of the triangle vertices is connected to other edges with $\varepsilon_d > \varepsilon_4$. This level of $G(x)$ separates in $G(y)$ two additional components of arcwise connectedness adjacent, respectively, to vertices 1 and 3. After connecting the point ε_4 to the end vertices 1 and 3, construction of the thermodynamic tree is completed.

Stages of the "growth" of such a tree for hydrogen combustion are shown in Fig. 4.4. The numbers ε_d of the edges of $D(y)$ are arranged as follows:

$$\varepsilon_3 < \varepsilon_1 < \varepsilon_6 < \varepsilon_2 < \varepsilon_4 < \varepsilon_5 < \varepsilon_8 < \varepsilon_7 < \varepsilon_{14} < \varepsilon_{13} < \varepsilon_9 < \varepsilon_{10} < \varepsilon_{12} < \varepsilon_{11} < \varepsilon_{15}$$

(the numbers of edges are presented in Fig. 4.4).

Because of the multidimensionality of the space ($n = 6$) in this case, as distinct from the description of the tree of hexane isomerization, we will sequentially represent graphically the removed edges of the graph $D(y)$ rather than the components corresponding to new branches of arcwise connectedness. Such graphical interpretation of tree growth is clear, since connection of each new branch to the tree means simultaneous substitution of some multidimensional region $D(y)$ by the one-dimensional segment. Disappearance of multidimensional regions leads to disappearance of the corresponding edges.

As in the previous case, construction will start with the root x^{eq}. We connect it with the least one among $\varepsilon_d - \varepsilon_3$. After removal of edge 3 the graph of the balance polyhedron remains connected. Hence, any two vertices of $D(y)$ can be connected with each other by an edge, a chain, or chains with max min ε_d on the parallel chains, max min $\varepsilon_d > \varepsilon_3$. The point ε_3 in this case is not a branch point. A similar situation is observed after removal of edges 1, 6, 2, and 4.

Only after rejection of edge 5 is the graph $D(y)$ broken into two components: the vertex H_2O and "the remainder." Then it becomes possible to draw two twigs of the tree: $x^{eq} - \varepsilon_5$ and $\varepsilon_5 -$ H_2O. The next tree growth (the branches $\varepsilon_5 - \varepsilon_{14}$ and $\varepsilon_{14} -$ H_2, O_2) is executed after removal of edge 14. After sequential removal of edges 13 and 9 the vertex H_2, OH is separated from the graph, and becomes a new endpoint of the tree. Then the new vertices appear, respectively, after removal of edges 12 (H, OH) and 11 (H_2, O). The tree construction is completed after removal of edge 15, leading to formation of two last components of arcwise connectedness that border on the vertices (H, O) and (H, O_2).

The first example of converting the balance polyhedron to a tree (for the isomerization reaction) can evidently be explained as a process of sequential removal of edges from the graph $D(y)$.

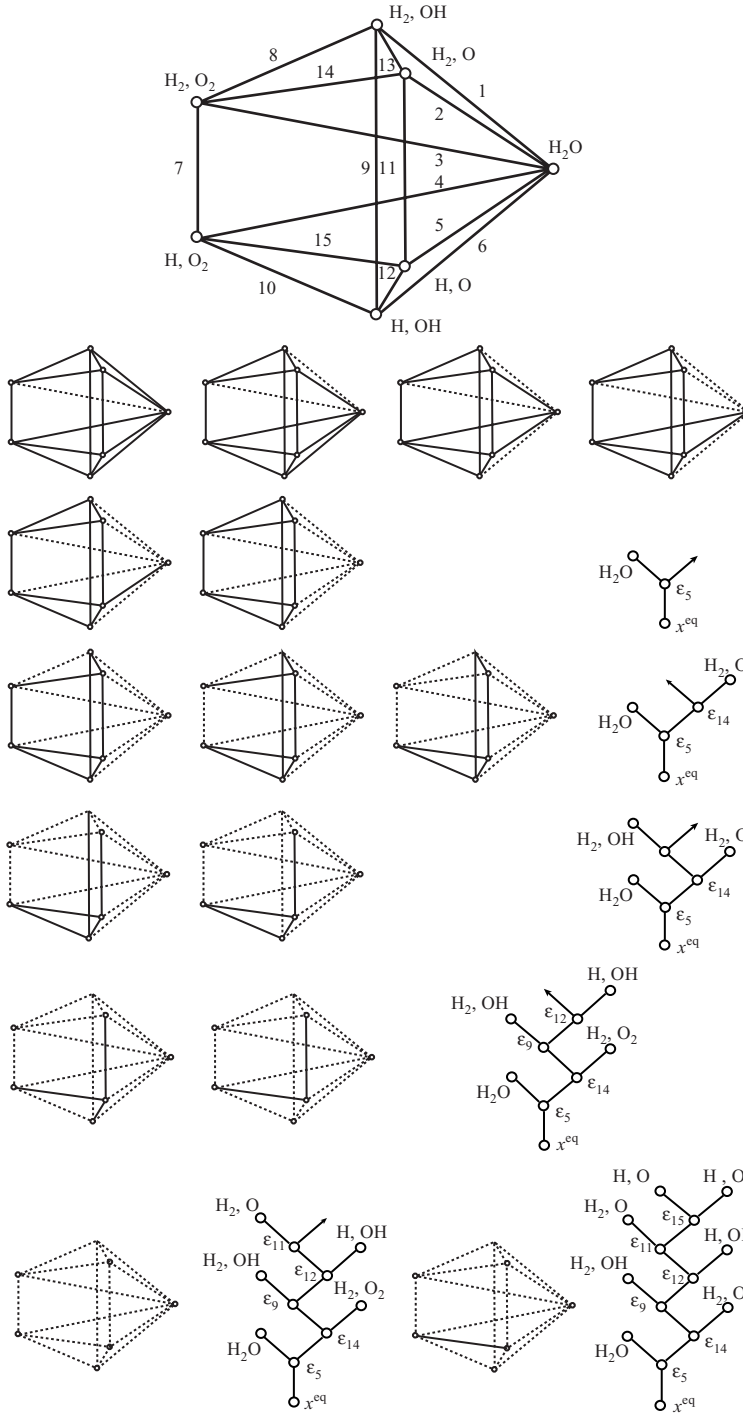

FIGURE 4.4. Construction of the thermodynamic tree for hydrogen combustion in oxygen.

After we have given graphical illustrations of the algorithm of tree construction, it is relevant to note that the equilibrium point x^{eq} can be a ramification point only at the one-dimensional $D(y)$, i.e., at $n - m = 1$. It is obvious that from the part of such a polyhedron to the left of x^{eq} we cannot reach the part to the right and vice versa. Therefore, both parts turn out to be different components of arcwise connectedness with respect to the equilibrium point.

Now we present a brief formal description of the exact algorithm of constructing a thermodynamic tree:

1. Construction of the graph of balance polyhedron $D(y)$.
2. Formation of the list of vertices of $D_0 = \{\upsilon_1, \ldots, \upsilon_l\}$.
3. Formation of the list of edges of $D_1 = \{d_1, \ldots, d_k\}$.
4. Calculation of the minimum values of $G(x)$ at the edges ε_d.
5. Arrangement of the values of ε_d in increasing order.
6. Calculation of the value of x^{eq} (by the affine scaling method, for example).
7. Connection of the point x^{eq} with the least ε_d.
8. Check of whether removal of the edge d results in separation of some vertex (vertices) υ from the polyhedron, i.e., whether ε_d is a ramification point.
9. If yes, connection of the ramification point ε_d to the vertex (vertices) υ and determination of the next tree branch (branches).
10. Check of whether ε_d is the highest level of ε . If yes, termination of the algorithm work.
11. Connection of the point ε_d to the next point ε (in order of increasing value) and transition to item 8.

The simplest examples presented in addition to the analysis in Section 3.2 illustrate an extreme complexity of the algorithm described. Apart from knowing the graph (remember that it can have an astronomic number of vertices), we need information about the Gibbs energy values at all the vertices and about the minimum values of $G(x)$ at all the edges prior to construction of the tree.

Possibilities for development of simplified numerical algorithms for constructing the tree that result in approximate solutions will be illustrated again with the example of isomerization (though, in this case, in a space of five variables). It is convenient to apply this example to a small-dimensional problem, because $D(y)$ as described by the single equation of the material balance is always a simplex and its graph is easily constructed by connecting each vertex with all the remainders.

A simplex of the process comprising mutual transformations of five isomers to each other is presented in Fig. 4.5*a*. It has 5 vertices (C_1^5) and 10 edges (C_2^5). If the minimum values of $G(x)$ at the edges are ordered as

$$\varepsilon_1 < \varepsilon_2 < \varepsilon_3, \ldots, < \varepsilon_9 < \varepsilon_{10}.$$

then the tree of this simplex takes the form presented in Fig. 4.5*b*. It is clear that the point ε_7 is the first (lower) ramification point, since the simplex with 5 vertices turns into a tree in which the number of edges is equal to 4.

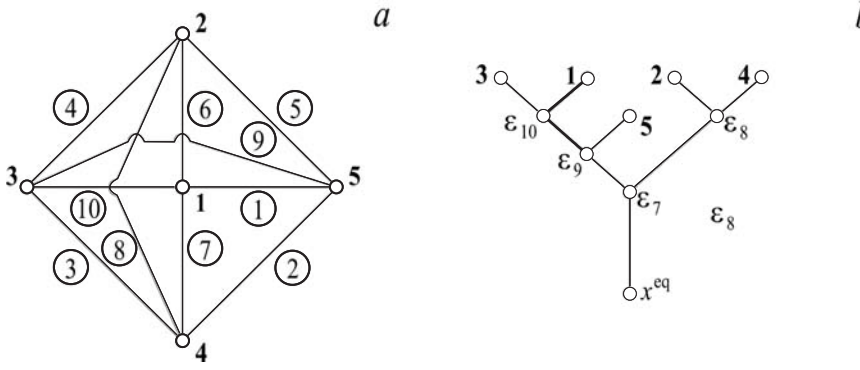

FIGURE 4.5. Simplex (*a*) and thermodynamic tree (*b*) of mutual transformations of five isomers.

If we assume that $y = (1, 0, 0, 0, 0)^T$, i.e., the initial state is represented by point 1 and the process goal is to obtain the maximum quantity of the fifth component, then the level ε_9 will be the surface level of $G = G(\max x_5)$.

Now we will try to find this level in accordance with the idea formulated in Section 3.2, constructing trees not for the whole polyhedron $D(y)$, but for its separate faces. Fig. 4.6 presents trees constructed for the three-dimensional faces, whose set D_0 contains vertices 1 (y) and 5 (x^{mat}). Using two trees from the obtained ones, we determine the same optimal level $G(x) = \varepsilon_9$ as we found in the tree of the whole simplex (Fig. 4.5). The trajectories of motion from y to $\max x_5$ along the tree branches are shown in Fig. 4.5–4.7 by bold lines.

If the trees are constructed at the two-dimensional faces with vertices 1 and 5, the optimal problem solution is also found in one of the three possible cases (Fig. 4.7).

Thus, these examples demonstrate the possibility for decreasing dimensionality of the problem of thermodynamic tree construction: substitution of the problem by one of determining projections of this tree on individual faces of the balance polyhedron. Even for complex real systems such substitution essentially decreases dimensionality of the problem of searching for the optimal level of $G(x)$ (or some other thermodynamic function). So, for the studied system with $n = 200$ and $m = 20$, the number of two-dimensional faces with two equal fixed vertices (y and x^{mat}) at the same edge makes up 179 (from $C_B^A = C_{178}^{179} = 179$, where A is the power of intersection of the sets of zero components at y and x^{mat} and B is the dimensionality of the set of zero components for the two-dimensional faces). Construction of about 200 trees for comparatively simple polyhedrons seems now to be a realizable problem.

Certainly it may happen that to determine $G(x^{\text{ext}})$, trees should be constructed at faces with dimensionality higher than 2.

To further analyze the idea on algorithm simplification two additional examples were considered: 1) combustion of pure carbon and 2) coal combustion in the air. To analyze both examples one and the same sequence of procedures was applied:

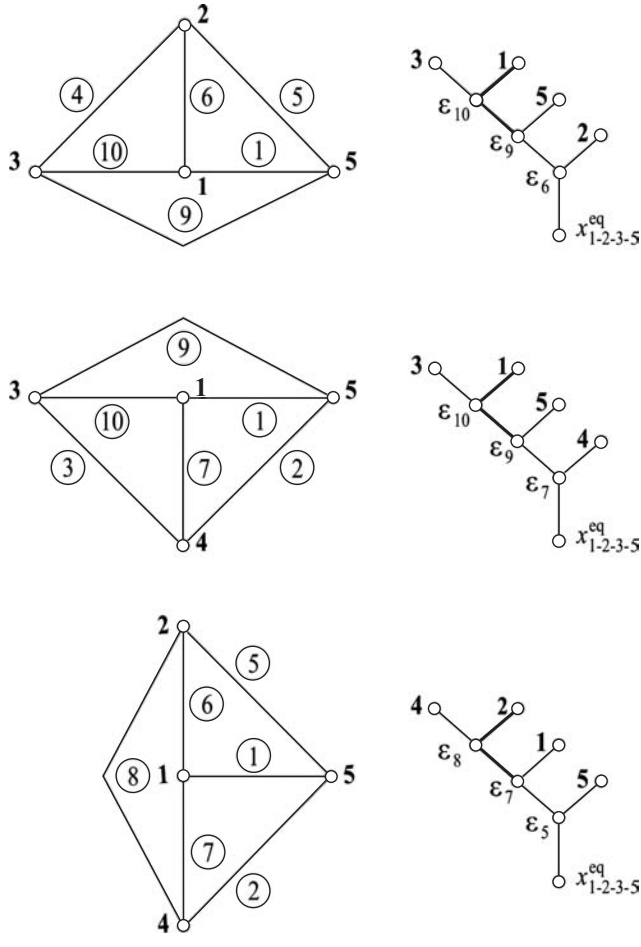

FIGURE 4.6. Three-dimensional faces of the simplex and the associated thermodynamic trees.

- The (intuitive) choice of a subset of solutions to the system of material balance equations, i.e., determination of part of the vertices of $D(y)$ (a subset of the set $D_0(y)$; in this case the choice of sample space necessarily included the vertices y (or the nearest one to y, if the initial system state does not coincide with one of the vertices of $D(y)$ and x^{mat} (the point of the maximum concentration of a given set of substances on $D(y)$).
- Application of the criterion

$$I_j \cap I_i = n - m - 1 \tag{4.45}$$

to check which segment connecting the determined vertices are the edges of $D(y)$ (here I_j and I_i are sets of indices of the zero components of x at the

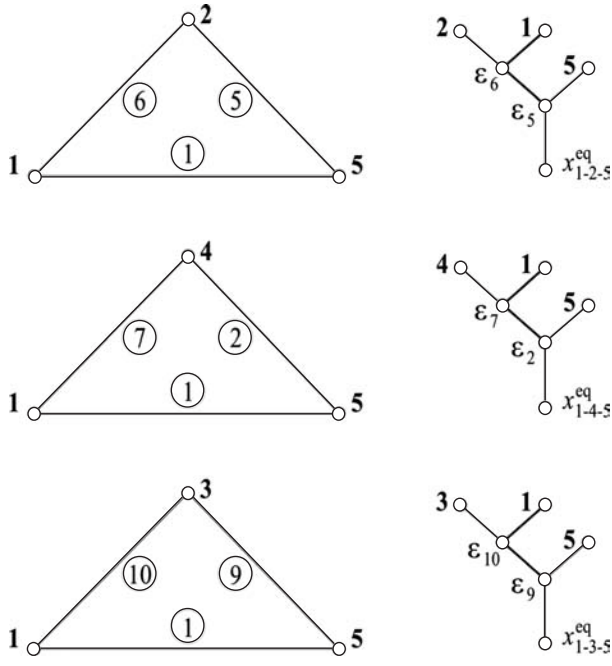

FIGURE 4.7. Two-dimensional faces of the simplex and the associated thermodynamic trees.

vertices j and i, respectively); then construction of a partial graph of the balance polyhedron (criterion (4.45) can be replaced by the criterion $I_j \cup I_i = m + 1$, where I_j and I_i are already sets of the nonzero components).

- Selection of connected parts of lower dimensionality (if possible) from the determined partial graph (preferably in the form of triangles) that contain the points y and x^{mat}.
- Construction of trees for the obtained parts and determination at them of the maximum ε_d on the thermodynamically admissible paths from y towards x^{mat}.

The solutions to the problem (searching for max ε_d for the considered examples) are interpreted by the plots in Figs. 4.8 and 4.9.

The graph with 7 vertices in Fig. 4.8*a* is part of the complete graph $D(y)$ of a system with 8 variables (x_{CO}, x_{CO_2}, x_{N_2}, x_{NO}, x_{NO_2}, x_O, x_{O_2}, x_C) and 3 material balances (for carbon, oxygen, and nitrogen) having 12 vertices. The vertices of the drawn graph correspond to maximum concentrations of substances forming a system.

Two triangular faces (Fig. 4.8*b* and *c*) and one quadrangular face (Fig. 4.8*d*) including the vertices y (7) and x^{mat}_{NO} (4) were separated from the graph in Fig. 4.8*a* to construct trees. In this case, in accordance with the problem conditions, $y = (y_{N_2} = 25.5; y_{O_2} = 6.8; y_C = 5.7)^T$ and $x^{\text{mat}}_{NO} = (x_{N_2} = 18.7;$

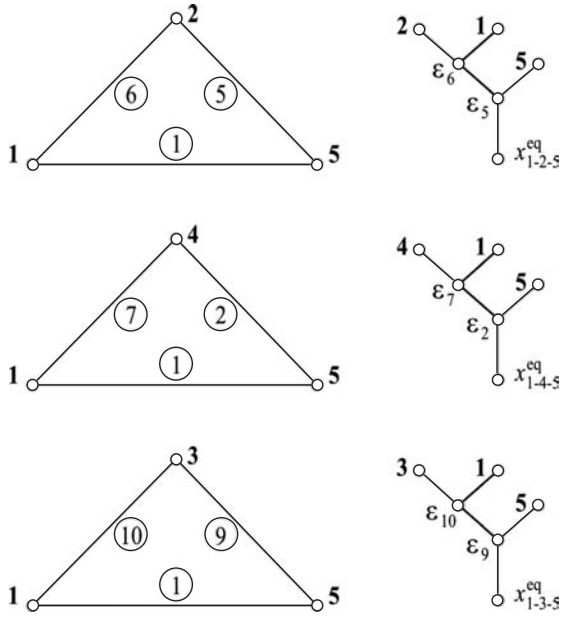

FIGURE 4.8. Construction of thermo-dynamic trees for carbon combustion reaction.

$x_{NO}= 13.6; x_C = 5.7)^T$. The same maximum value of $\varepsilon_d = -15.207$kJ was determined with the help of each the constructed tree (in Fig. 4.8 and 4.9 the values of $G(x)$ are given on the edges of polyhedrons and at the points of tree branching). This value turned to be somewhat higher than that determined by E.G. Antsiferov's [4, 7, 8] approximate algorithm (-15.211).

Though the graph in Fig. 4.9*a* is not more complex in structure than the graph in Fig. 4.8*a*, it belongs to a much more complex system. Coal combustion was modeled by the system comprising 23 components (CH_4, CN, CN_2, CO, CO_2, H, H_2O, H_2O_2, HO_2, N, N_2, N_2O, NH, NH_3, NO, NO_2, O, O_2, O_3, OH, SO_2, C, coal) and satisfying 5 material balances (for carbon, oxygen, nitrogen, hydrogen, and sulfur). Coal was represented by the conditional molecular formula: $CH_{0.833}O_{0.233}N_{0.012}S_{0.002}$.

The graph (Fig. 4.9*a*) was obtained from another partial graph containing 23 vertices by elimination from the latter those edges that did not belong to the triangular faces including the vertices y (23) and x_{NO}^{mat} (15). The tree of the triangular face 12–15–23 determined the level of $G(x)$ that corresponded to the maximum concentration of NO (-15.571 kJ) and coincided with that obtained by Antsiferov's algorithm.

Thus, two last examples also confirmed the efficiency of simplified algorithms for constructing a thermodynamic tree. More accurate values of $G(x^{ext})$ obtained in some examples than what was obtained by Antsiferov's algorithm raise hopes for the effective application of such algorithms.

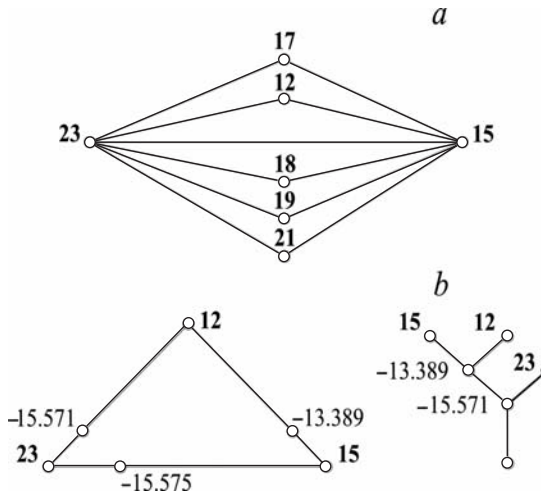

FIGURE 4.9. Construction of thermodynamic trees for coal combustion reaction.

The computational procedures describing two last examples may surely be considered only as drafts of these algorithms.

Their creation calls for further theoretical comprehension of the problem and practical tests of the outlined computational approach. Formalization of the problem of searching for the partial graphs for which thermodynamic trees are constructed will apparently be central in development of the approach.

4.5. Analysis of Feasibility and Stability of Partial Equilibria

The most difficult and frequent questions among those arising in MEIS application are the following: "How complicated is it, and is it possible in general to implement the determined extreme state?" and "Is this state maintained long enough to extract or register the target products?" In many cases the positive answer is suggested by the available experience of studying processes similar to the considered one. Possibilities for production of hydrocarbons, these being intermediate products of fuel processing discussed in the final chapter (Chapter 5) of the book, are confirmed, for example, by operating data of numerous technological installations. Experiments also reveal the presence of harmful substances in the atmosphere, whose calculated extreme concentrations are presented in Section 5.1.

However, in the analysis of new technologies that were not tested experimentally and in the calculations of poorly studied processes of environmental pollution, the response to the question on feasibility of extreme partial equilibria is not known

in advance. Along with the question on duration and retainability[2] of the sought states the question often arises of their stability in the face of different disturbances, such as changes in initial composition, pressure, temperature, and so on.

This section presents preliminary considerations on possible algorithms of analysis performed after calculations on MEIS; our aim is to estimate the achievability (realizability) of determined intermediate extreme states. We suppose that the described sketch of the technique variant for such an analysis will find application to further studies on stability and retainability of partial equilibria.

The key premise consistent with the preliminary nature of subsequent reasoning is that the considered thermodynamic system is closed and, hence, does not comprise processes of matter and energy transit throughout the system. Such processes were discussed in Chapter 6 of *Equilibrium Encircling* (see Section 1.5).

The first stage of the analysis on achievability of the state x^{ext} should certainly entail checking its stability. To do this, first of all it is necessary for us to choose "suspicious" chemical reactions, ones whose rates may turn out to be high enough for the system to move in a short period of time by a considerable distance from the partial equilibrium determined by MEIS. Here one should take into account possible formation of active particles in the process of reaching x^{ext}, which can stimulate further conversions of substances. A list of "suspicious" reactions can be used sometimes for an aggregate description of the entire studied process from initial state y to reactions proceeding after the sought extreme point is passed.

Reactions can be written in the conventional kinetic form, i.e., with the help of derivatives of concentration with respect to time, or in thermodynamic form (1.88), (1.101), as when rates are represented as functions of thermodynamic potentials. In the latter case the check of conditions for coordination (1.93) and balancing (1.94), which can also be described by inequality (1.95), appears useful in the retainability analysis of the state x^{ext}.

If the rate of chosen reactions proves to be high enough, it can be concluded that the determined x^{ext} is not achievable or that it should be provided by some artificial means (the sharp decrease of process temperature at the required instant, selection of catalysts, etc.).

The kinetic analysis of the retainability of x^{ext} will be illustrated on two examples. Hexane isomerization, which was handled many times above in all its aspects, will be the first example. Let us turn again to Fig. 3.1. Suppose that only monomolecular reactions are possible at the point $x_2^{\text{ext}} = (0.075, 0.860, 0.065)$:

1) $x_1 \to x_3$,
2) $x_2 \to x_3$,
3) $x_2 \to x_1$.

[2] Here we use the word "retainability" to express the ability of extreme states to preserve over time—distinct from their ability to be reached at a variation of some conditions, i.e., stability.

TABLE 4.2. Methane pyrolysis at one volume percent of air at $T = 1273$ K and $P = 0.1$ MPa. Substance concentrations, mole/kg

Substance	Initial composition	Composition in 2 hours	Equilibrium composition	$x^{\text{ext}}_{C_2H_2}$	
				kinetic	thermodynamic
C_2H_2		**$3.637 \cdot 10^{-3}$**	**$4.898 \cdot 10^{-5}$**	**8.471**	**21.76**
C_2H_3		$1.353 \cdot 10^{-9}$	$1.248 \cdot 10^{-8}$	$9.901 \cdot 10^{-7}$	$9.332 \cdot 10^{-9}$
C_2H_4		$7.021 \cdot 10^{-6}$	$1.892 \cdot 10^{-4}$	$1.514 \cdot 10^{-2}$	$1.283 \cdot 10^{-4}$
C_2H_5		$1.535 \cdot 10^{-10}$	$1.013 \cdot 10^{-8}$	$1.052 \cdot 10^{-7}$	$6.225 \cdot 10^{-9}$
C_2H_6		$3.650 \cdot 10^{-6}$	$1.273 \cdot 10^{-5}$	$6.668 \cdot 10^{-3}$	$7.094 \cdot 10^{-6}$
CH_2		$6.749 \cdot 10^{-15}$	$7.322 \cdot 10^{-12}$	$3.934 \cdot 10^{-14}$	$6.038 \cdot 10^{-12}$
CH_3		$1.062 \cdot 10^{-5}$	$1.673 \cdot 10^{-5}$	$3.514 \cdot 10^{-4}$	$1.251 \cdot 10^{-5}$
CH_4	**61.07**	**0.9185**	**1.139**	**36.12**	**0.7719**
CO		$2.372 \cdot 10^{-2}$	0.2313	$3.092 \cdot 10^{-2}$	0.2318
CO_2	1.753E-4	$2.830 \cdot 10^{-5}$	$3.176 \cdot 10^{-6}$	$7.321 \cdot 10^{-3}$	$3.180 \cdot 10^{-6}$
H		$5.419 \cdot 10^{-5}$	$8.593 \cdot 10^{-5}$	$1.702 \cdot 10^{-5}$	$7.815 \cdot 10^{-5}$
H_2		**118.24**	**119.9**	**44.10**	**98.83**
H_2O		0.2104	$2.750 \cdot 10^{-3}$	0.1886	$2.265 \cdot 10^{-3}$
H_2O_2		$8.103 \cdot 10^{-19}$	0	$2.580 \cdot 10^{-16}$	0
HCO		$5.847 \cdot 10^{-7}$	$7.813 \cdot 10^{-10}$	$2.144 \cdot 10^{-7}$	$7.099 \cdot 10^{-10}$
O_2	0.1169	$1.481 \cdot 10^{-20}$	0	$1.417 \cdot 10^{-13}$	0
OH		$1.184 \cdot 10^{-9}$	$2.257 \cdot 10^{-11}$	$5.068 \cdot 10^{-10}$	$2.051 \cdot 10^{-11}$
C (cond.)		**60.12**	**59.70**	**7.924**	**16.55**

Note: The inert components x_{Ar} and x_{N_2} are not shown.

It is clear that the processes leading to an increase in concentration of the component x_2 cannot start from the point x_2^{ext}, since the Gibbs free energy increases in this case.

After obvious transformations of equation (1.101) the rate of the above stages (e.g., the third) will have the form

$$w_s = k\left(e^{-\frac{\mu_2^0}{RT}} e^{m_2} - e^{-\frac{\mu_1^0}{RT}} e^{m_1}\right).$$

Since the rate constants k of monomolecular reactions have an order of 10^{13}–10^{14} s^{-1} [135], it is easily seen that the numerical value of w_s is extraordinary high and hence, the state x_2^{ext} will be unstable (inretainable).

The methane pyrolysis process aimed at acetylene production, which was studied in [99], was taken as the second example. The calculation results of this process are presented in Table 4.2 and Fig. 4.10. The most important components are presented in the table in bold typeface.

The computational experiment was based on the formal kinetic description of 95 reactions with participation of 25 substances. The calculated partial equilibrium (the column "$x^{\text{ext}}_{C_2H_2}$ kinetic" in Table 4.2) can be interpreted to correspond to the extreme concentration of C_2H_2 at the existing kinetic constraints. The acetylene concentration in it turned out to be approximately 2.5 times lower than at the thermodynamically attainable state, where there are no kinetic constraints (the column "$x^{\text{ext}}_{C_2H_2}$ thermodynamic").

FIGURE 4.10. Calculation of methane pyrolysis.

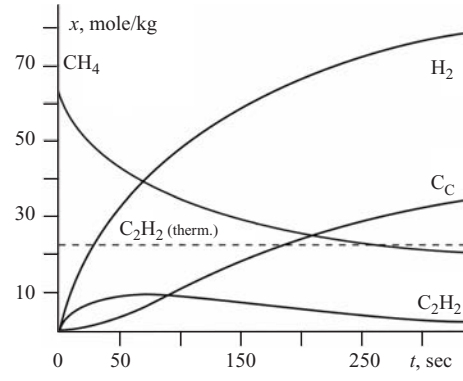

Table 4.2 and Fig. 4.10 show that in this case, the extreme state displays retainability probably sufficient for extraction of the desired process product from the reactor. Approximately for a minute after the extremum point is reached, concentration of C_2H_2 does not vary essentially.

If an extreme state obtains for a noticeable amount of time, then it is necessary to evaluate its stability, to check the feasibility of a sharp decrease in retainability as a result of possible disturbances of the process or change of the extreme point position with the corresponding change in concentrations.

Strict physical and mathematical formulations of the problems to be solved are also complicated at the present time. Thus, the feasibility and expediency of describing these problems in terms of stability theory are far from obvious. Indeed, in traditional formulations of the problem where we are searching for global thermodynamic equilibrium in closed systems with equilibrium environment, we deal with Lyapunov functions tending to the stationary point (the point of system's stable equilibrium). All possible trajectories in the thermodynamic attainability region $D_t(y)$ are usually stable. It becomes senseless to apply criteria and methods to check this fact.

It may be apparently reasonable to employ a technique of the stability theory, but only when some nonthermodynamic factors that distinguish particular admissible directions of motion in $D_t(y)$ are taken into account. Such factors may include retardation of all possible physicochemical processes after the point x^{ext} is reached; or limitation of the reaction mechanism by several basic stages, as we presented in the above example of isomerization.

When we analyze the impact of disturbances on solutions obtained by MEIS, it seems most simple and logical to initially estimate sensitivity of these solutions. This may be the second step of the algorithm for determination of properties of the found extreme intermediate state.

At the first stage of this step, in turn, the presumably most dangerous disturbances for this specific case should be chosen (changes in the initial data of MEIS). Disturbances may occur due to deviations from the accepted initial values of the vector y, the environmental temperature and pressure, and other factors. Variations

in the raw material quality (e.g., the composition of fuel burnt in boiler furnaces) is a typical reason for change in technological systems. In natural objects such changes can be caused by nonstationary meteorological conditions or unstable anthropogenic loads.

The sensitivity analysis for the selected disturbances can be most easily performed by variant calculations on MEIS, determining, for example, the functions $\Delta x^{\text{ext}} = f(\Delta y)$, where Δx^{ext} and Δy denote changes in the values of the vectors x^{ext} and y with respect to the basic calculated variant.

In the sensitivity analysis the use of the thermodynamic tree may prove to be highly useful. Let us turn again to Fig. 3.1. It is easily seen how the optimal level of the Gibbs energy $G = G(x^{\text{ext}})$ changes as a function of $y$when searching for the maximum concentration of the third component (x_3^{ext}) of the reaction mixture. At $y = (1, 0, 0)^T$ (vertex 1) this level is equal to -424.118 kJ, and at $y = (0, 1, 0)^T$ (vertex 2) it is -425.678 kJ (Fig. 3.1*b*). The values of x_3^{ext} change correspondingly (Fig. 3.1*a*).

The last (third) step of the mentioned technique consists apparently in the stability analysis itself. Some preliminary considerations can also be applied to this analysis. For example, it is preferable to use the first (direct) Lyapunov method, since the type and properties of the studied functions are known to a considerable extent beforehand. However, more detailed representation of suppositions on the contents of the third step is premature yet. In order to exactly formulate the problem solved at this stage we need a sufficient experience in the study on properties of extreme partial equilibria.

In conclusion we note that, after the problem of estimating the properties of extreme states in closed systems is solved successfully (we look to the success), it is necessary to analyze specific features of MEIS-based solutions for open systems. These are, first of all, cases in which transit flows of energy make up an essential portion of the converted energy in the system, and where modeling of real open systems by closed ones can lead to significant errors. Here it is convenient to take advantage of the approach developed in Chapter 6 of *Equilibrium Encircling* [58] (see Section 1.5).